American Mineralogist, Volume 77, pages 911–922, 1992

The structure of hematite {001} surfaces by scanning tunneling microscopy: Image interpretation, surface relaxation, and step structure

CARRICK M. EGGLESTON*
Department of Applied Earth Sciences, Stanford University, Stanford, California 94305-2225, U.S.A.
MICHAEL F. HOCHELLA, JR.
Department of Geology, Stanford University, Stanford, California 94305-2115, U.S.A.

ABSTRACT

Scanning tunneling microscopy (STM) is used to study the structure of {001} hematite single-crystal surfaces. STM images taken at negative sample bias consistently show a hexagonal array of atomic sites with 3-Å periodicity, as expected for the surface O array and in agreement with photoelectron spectroscopy studies of hematite surfaces after O_2 and H_2O exposure which show that states at the top of the valence band have O character. Molecular orbital calculations suggest that these states are localized on O sites. In contrast, STM images taken at positive sample bias were variable, sometimes showing hexagonal arrays with O periodicity and sometimes showing arrays with equivalent Fe periodicity. Moreover, because the states at the base of the conduction band are not necessarily localized on atomic sites, the STM images taken at positive sample bias may not show atomic positions.

With the above findings in mind, we used negative bias images to study relaxation of O positions on the hematite {001} surface. Surface O positions are apparently relaxed to a regularized hexagonal array with a single-mode distribution of O-O interatomic distances; in the equivalent bulk plane, O-O distances form a bimodal distribution because of distortion by octahedral face sharing across the (001) plane.

STM images also show that step densities on hematite {001} fracture surfaces are high, often one step every 20–30 Å. The atomic structure near step edges appears to be reconstructed relative to terraces, but convolution of atomic and electronic structure information in STM images makes precise interpretation of step structure difficult.

INTRODUCTION

Many geochemically important reactions occur at mineral surfaces and are strongly influenced by surface atomic and electronic structure (e.g., see Hochella, 1990). These structures determine the variety and nature of bonding environments and energetic pathways available to reactants as they adsorb, diffuse across the surface, and participate in surface reactions. In general, the structure of a solid surface differs from that of a simple bulk termination. Surface reconstruction refers to a surface reorganization that results in a surface unit cell of different size (and often symmetry) from that of the equivalent bulk plane. Reconstruction usually involves the breakage and formation of bonds, and activation energies for reconstruction are therefore relatively high. Surface relaxation refers to slight displacements of surface atoms in response to force asymmetries at the surface; the surface unit cell remains nearly unchanged (e.g., Hochella et al., 1990; Hochella, 1990; Brown, 1990). In general, all surfaces relax to some extent (Somorjai, 1981).

An example of surface reconstruction is the technologically important Si (111) 7 × 7, whose surface unit cell is seven times larger along both axes than the unreconstructed cell, hence "7 × 7." In vacuum, this reconstruction reduces the number of dangling bonds at the surface from 49 to 19 per unit cell. Surface energy is thus minimized by satisfaction of dangling bonds; dangling bonds may also be satisfied by chemisorption (for a geologic example, see Parks, 1984). In contrast, surface relaxation reduces surface energy because surface atoms adjust to minimum potential energy positions within the asymmetric force environment at the surface.

Direct probing of surface structure can thus lead to new understanding of reaction mechanisms (e.g., Eggleston and Hochella, 1991) as well as of the thermodynamics of surfaces (e.g., Williams and Bartelt, 1991); that is, we may study the microscopic structural basis for properties previously only observed indirectly. For example, surface or interfacial energy (a thermodynamic property) is a crucial part of theories concerned with the nucleation of new phases (e.g., Zhang and Nancollas, 1990), the nucleation of etch pits (Lasaga and Blum, 1986; Brantley et al., 1986), and brittle fracture (Lawn and Wilshaw, 1975). Ther-

* Present address: Swiss Federal Institute of Technology, EAWAG/ETHZ, CH-8600 Dübendorf, Switzerland.

0003–004X/92/0910–0911$02.00

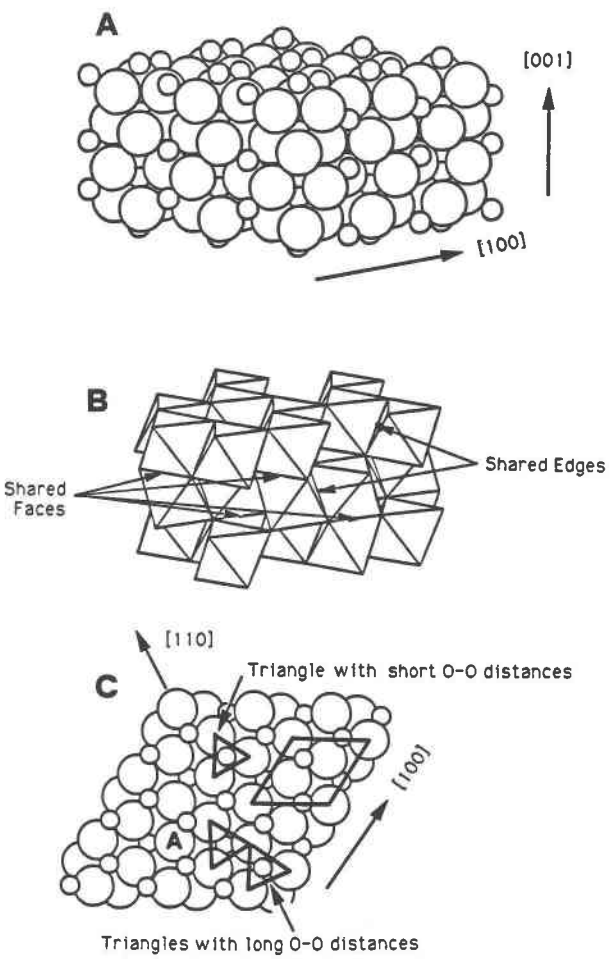

Fig. 1. (A) A model of a segment of the bulk hematite structure (calculated from the refinement of Blake et al., 1966). Crystallographic directions are indicated. O layers alternate with Fe layers in the [001] direction. High-Fe atoms on the {001} surface sit above shared octahedral faces, and low-Fe atoms sit above unshared faces. (B) Polyhedron model of the hematite bulk structure. Several face-sharing and edge-sharing octahedra are marked. (C) The hematite structure projected on {001}. A surface unit cell, corresponding in size to the bulk unit-cell face in the {001} plane, is drawn so as to connect equivalent O positions. Three O triangles are indicated with connecting lines to illustrate the occurrence of large and small O triplets within an O plane. The site marked A is referred to in Figure 6.

modynamic discussions of solid surface energies may be found in Jaycock and Parfitt (1981), Adamson (1982), and Parks (1990), and treatments relating simple surface atomic structures to surface energies may be found in Benson and Yun (1967), Giese (1974), and Sparnaay (1985).

In this paper, we report the results of a scanning tunneling microscopy (STM) study of the atomic structure of hematite {001} surfaces, including interpretation of STM images taken under various imaging conditions, evidence for surface relaxation, and indications of reconstruction along step edges. Iron oxides and oxyhydroxides are of interest because they are ubiquitous in nature and may often influence natural H_2O chemistry (e.g., Schwertmann and Taylor, 1977; Bolt and Van Riemsdijk, 1987; Stumm and Sulzberger, 1992). They are particularly important in natural redox processes (e.g., Waite, 1990), and their redox and photoredox reactivity is a strong function of surface atomic and electronic structure (Leland and Bard, 1987). Hematite redox activity has led to interest in hematite electrodes for industrial purposes (e.g., Kurtz and Henrich, 1983; Henrich, 1985). From a purely structural point of view, hematite is an interesting material because its bulk structure contains distorted edge- and face-sharing octahedra, suggesting the possibility of significant surface relaxations.

Hematite structure

Bulk structure

The bulk hematite structure may be thought of as a hexagonally closest-packed array of O atoms, with Fe atoms in two-thirds of the octahedral sites. Figure 1A shows a section of bulk structure in which O layers alternate with layers of Fe along [001]. The high-Fe atoms on the (001) face of Figure 1A are above O triplets that constitute a shared octahedral face with the next layer down; Fe-Fe repulsion causes these Fe atoms to move as far away from the shared face as possible. The low-Fe atoms are above unshared faces (vacancies in the layer below). Figure 1B illustrates some face-sharing, edge-sharing, and vacant octahedra. This face and edge sharing causes substantial distortion of the ideal hexagonal closest-packed structure (Lindsley, 1976). Specifically, the three O atoms of the shared octahedral face move closer together than they would be in an ideal octahedron, and the O atoms of the unshared faces move farther apart. Therefore, within a single (001) O plane (see Fig. 1C), two large O triangles (edge length 3.035 Å) alternate with single small O triangles (edge length 2.669 Å). The Fe-O bond lengths are 1.945 Å to the unshared face and 2.116 Å to the shared face. These may be compared with an Fe-O distance of 2.06 Å for maghemite (Fasiska, 1967), which has nearly ideal octahedral site geometry (Lindsley, 1976; Sherman, 1985); Fe-O bonds in hematite are strained relative to this "unstrained" Fe-O distance.

Surface structure

Hematite parts along {001}. During fracture, the {001} plane provides a pathway along which only long Fe-O bonds need be broken (Kurtz and Henrich, 1983; Johnsson et al., 1991). If this occurs, the Fe atoms bonded to the unshared faces (the low-Fe atoms in Fig. 1A) are left behind, creating a polar surface; that is, the top layer of atoms on each of the opposing fracture surfaces consists entirely of positive charge. This, together with the strained nature of the bulk structure, is thought to provide a large driving force for chemisorption, relaxation, or reconstruction (Henrich, 1985; Pisani et al., 1987).

Few studies have been made of the hematite {001} surface structure. Kurtz and Henrich (1983) used low-

energy electron diffraction (LEED) and X-ray photoelectron spectroscopy (XPS) to study hematite {001} in ultrahigh vacuum (UHV) after ion sputter cleaning and annealing at 700 and 820 °C. Their surface treatments produced an O-deficient surface containing Fe^{2+} and Fe^0 in addition to Fe^{3+} and exhibiting 2×2, $\sqrt{3} \times \sqrt{3}R30°$ (R = rotated), and "complicated incommensurate" reconstructions. These structures result from sputtering and annealing in UHV (with loss of O from the surface) and probably do not exist under ambient conditions (Kurtz and Henrich, 1983). Hochella et al. (1989) studied hematite {001} by LEED at room temperature, without pretreatment, and found an unreconstructed 1×1 surface. Heil et al. (1989) imaged hematite with STM at room temperature and described the results as consistent with the structure expected from a bulk termination (i.e., 1×1), although details of interpretation were not addressed (see below). Johnsson et al. (1991) studied hematite {001} surfaces with both STM and scanning force microscopy (SFM) and found a 1×1 surface structure (see below).

Alumina (α-Al_2O_3) is isostructural with hematite and is more extensively studied because of its importance as a catalytic support and as a template for the epitaxial growth of Si. Charig (1967) and Chang (1968), using LEED, found unreconstructed surfaces for unheated samples. Heating over 900 °C produced either a $\sqrt{3} \times \sqrt{3}R30°$, a $3\sqrt{3} \times 3\sqrt{3}R30°$, or a $\sqrt{31} \times \sqrt{31}R \tan^{-1}(\frac{5}{11})^{1/2}$ reconstruction. Heating over 1400 °C produced $\sqrt{31} \times \sqrt{31}R \tan^{-1}(\frac{5}{11})^{1/2}$ structure over the entire surface. French and Somorjai (1970) found similar results, attributed the reconstructions to surface nonstoichiometry (O_2 was detected by mass spectrometry during heating in UHV), and suggested that isostructural compounds might behave similarly (this prediction is at least partially confirmed for hematite by Kurtz and Henrich, 1983). Susnitzky and Carter (1984) found evidence for a $\sqrt{3} \times \sqrt{3}R30°$ surface structure in TEM studies of thin α-Al_2O_3 films; the reconstruction probably resulted from electron beam heating.

The available information on α-Fe_2O_3 and α-Al_2O_3 {001} surface structures suggests that an unreconstructed 1×1 surface structure should be stable up to 700 °C on hematite in UHV. The 1×1 structure is stable to even higher temperatures in air; Charig (1967) found that heating α-Al_2O_3 to 1250 °C in air did not reconstruct the surface. None of these studies attempted to determine surface atomic positions; surface relaxation on hematite {001} and α-Al_2O_3 has, to our knowledge, never been experimentally examined.

Several theoretical studies have been made of surface relaxation on α-Al_2O_3 {001}. Pisani et al. (1987) used a molecular orbital (MO) approach and a slab model of the surface in which only relaxation of the surface Al atoms parallel to the [001] direction was considered. They found a 0.4-Å relaxation of the surface Al atoms toward the first O layer (in effect, their calculation predicts that surface Al becomes embedded in the first O layer to form a charge-balanced surface). Causa et al. (1989) extended the results of Pisani et al. (1987) and found 0.4-Å relaxation of first-layer Al toward the surface, with a 26% reduction in surface energy relative to the unrelaxed surface.

None of the experimental or theoretical studies of α-Fe_2O_3 and α-Al_2O_3 {001} consider the possibility of surface relaxation within the {001} plane or of relaxation of O atoms in the [001] direction. Also, most of the studies mentioned above apply only to UHV; the threefold-coordinated-surface Al atoms in the theoretical studies (together with the surface energy and relaxation calculated for this configuration) would not be expected to exist under ambient conditions. Because STM can be used in air or under fluids, our results extend the studies mentioned above to conditions more closely approximating those under which hematite surfaces would participate in geochemical reactions.

Electronic structure

Molecular orbital (MO) calculations have been made for FeO_8^{9-} clusters by Tossell et al. (1973, 1974), Debnath and Anderson (1982), and Sherman (1985). These calculations suggest that the highest occupied molecular orbitals (HOMOs) in hematite-like clusters are crystal-field orbitals with substantial Fe 3d character and that states with O 2p character occur just below these HOMOs and are localized on O sites. The lowest unoccupied MOs (LUMOs) have mixed Fe and O character and are spatially diffuse (Tossell et al., 1974), with substantial state density in the interatomic region. The HOMOs and LUMOs of these cluster calculations would spread into bands in the bulk solid.

Valence band photoelectron spectra of hematite {001} surfaces are found in Tossell et al. (1973), Henrich (1985), Hendewerk et al. (1986), and Kurtz and Henrich (1987). By varying the O content of hematite surfaces by sputtering, annealing, and exposure to O_2, Kurtz and Henrich (1987) show that an Fe-related surface state lies at the top of the valence band, within the bulk band gap, and that states with O character lie below this state. Because STM is sensitive to the electronic states closest to the Fermi level (E_F), surface states play an important role in imaging. Kurtz and Henrich (1987) show that exposure of hematite {001} surfaces to O_2 depopulates the Fe-related surface state, leaving states with O character at the top of the valence band.

This situation may be rationalized by considering the creation of a hematite (001) surface by fracture in vacuum; the newly created surface has threefold-coordinated Fe in the first layer (Fe is sixfold coordinated in bulk) and threefold coordinated O in the second layer (O is fourfold coordinated in bulk; see Fig. 1C). Changes in electrostatic site potential because of coordinative undersaturation at the surface will stabilize or destabilize states in energy, creating surface states. Because surface Fe is less bulklike than surface O for the fresh (001) surface in vacuum, the surface states are likely to be mostly Fe related, as observed by Kurtz and Henrich (1987). However, in air or H_2O, surface Fe and O would be recoordinated by H_2O, O_2, OH^-, etc. Fe sites would regain octahedral coordination, except for asymmetry caused by differences in Fe

bonding to O in sorbate species (e.g., H_2O). Presumably, surface O dangling bonds would also be satisfied by chemisorption but not by bonding to Fe atoms as in the bulk. The most likely adsorbate would be H atoms in, or dissociated from, H_2O molecules (see Hendewerk et al., 1986; Kurtz and Henrich, 1987). Thus, after chemisorption of species from air, we might predict that surface O sites would be less bulklike than Fe sites and that surface states would most likely have O character. These states would correspond to partially satisfied O 2p dangling bond states at the surface, localized on O sites. Waite (1990) suggests that for a relatively ionic crystal such as hematite, surface states below E_F are indeed most likely to have anionic character, whereas surface states above E_F are likely to have cationic character. This overall result is in agreement with the photoelectron spectra discussed above for hematite surfaces after O_2 and H_2O exposure.

Experimental

Samples

Large, specular hematite crystals from Minas Gerais, Brazil, were obtained from the Stanford Mineral Collection. Samples were fractured along the (001) parting plane in air, and suitably flat surfaces were used for STM imaging. All imaged surfaces had been exposed to air for at least several hours. Hematite is an extrinsic semiconductor; charge carriers are contributed by impurities in the natural samples, and hematite can be either n or p type (Shuey, 1975; Waite, 1990). We have not determined whether our samples were n or p type, but we predict that they are p type: XPS of fresh {001} surfaces showed the expected composition and Fe oxidation state, and minor Mn impurities were found that would be expected to create holes in the valence band.

Tunneling microscopy

STM has been reviewed elsewhere (e.g., Hochella et al., 1989; Avouris, 1990; Eggleston and Hochella, 1990). Briefly, a very sharp metal tip is piezoelectrically scanned over a conducting or semiconducting sample surface, close enough (approximately 10 Å) for overlap of tip and sample electron density. Electrons can tunnel across the tip-sample gap, and when a small bias voltage (V_B) is applied a net tunneling current (I_T) can be measured. The constant-height imaging mode is used for atomic-resolution imaging in this study because it requires little mechanical response, often resulting in less noisy images. Thus, in the gray-scale images, dark areas represent low I_T and light areas represent high I_T. A feedback loop keeps the average I_T as close as possible to a user-defined setpoint current, I_{Tset}. In effect, the tip-sample separation is kept nearly constant.

STM images show essentially the local density of states (LDOS) near E_F at the surface (e.g., Avouris, 1990). The bias voltage and its polarity determine which states of the sample are imaged. In this study, bias voltage is applied to the sample; negative V_B causes electrons to tunnel from occupied sample states to the tip, and positive V_B causes tunneling from the tip to unoccupied sample states.

STM imaging was accomplished using a Digital Instruments Nanoscope II. W tips were made by electrochemical etching in 1 *M* KOH. Specific imaging conditions (V_B, I_{Tset}) are given in the figure captions. Samples were imaged under polyphenyl ether, a high molecular weight, nonpolar oil; nonconductive oils do not appear in or interfere with atomic-resolution STM images (Schneir and Hansma, 1987; Hochella et al., 1989). Imaging under oil often results in less noisy images, perhaps by minimizing ionic leakage currents.

The images presented below show effects of thermal and piezoelectric drift, effects which are ubiquitous in STM imaging. Drift causes nonorthogonality in the tip raster pattern and results in artifactual distortion of the atomic arrangement. Drift effects are usually obvious because they vary in a systematic way with scan direction and rate. Drift effects, together with vibrational noise and piezoelectric calibration errors, make determination of atomic positions and atom-atom distances from STM images inexact. However, if one has drift-independent information about the size and symmetry of the surface unit cell, drift effects can be accounted for. LEED by Hochella et al. (1989) shows that the hematite surface unit cell has a size and symmetry that is within error of the bulk unit cell in the {001} plane. Thus we may safely assume that the apparent distortions in unit-cell size and symmetry in the STM images are drift effects. As we shall discuss, however, the arrangement of atoms within the surface unit cell may differ from that in the equivalent bulk plane.

Results and discussion

Image interpretation

Figure 2 shows two examples of STM images of a hematite {001} surface taken at −300 mV V_B, conditions under which electrons tunnel from occupied valence band (or surface) states into the tip; a surface unit cell corresponding to the bulk (001) plane (Fig. 1C) has been superimposed on these images. There are peaks at each corner of the cell and two peaks entirely within it; these peak positions correspond approximately (but not exactly, as we discuss below) to O positions in the model cell (Fig. 1C). Fe sites do not occur in the pattern observed in Figure 2. Many images were taken under negative V_B conditions, using various samples and tips, and all consistently showed arrays similar to those in Figure 2.

If any Fe atoms lie above the O planes imaged in Figure 2, they are not imaged. Although UV photoelectron spectroscopy (UPS) studies of the hematite {001} surface in UHV show an Fe-related surface state at the top of the valence band (Kurtz and Henrich, 1987), the electronic structure in air or H_2O is likely to differ from that in UHV because of O or H_2O chemisorption (i.e., sorbate-induced surface states; see above). Fe exposed at the surface would not remain threefold coordinated but would chemisorb H_2O, O, and other molecules from the air to satisfy dan-

gling bonds (e.g., see Parks, 1984; Hochella, 1990). H_2O initially sorbs to hematite {001} dissociatively but sorbs without dissociation at higher coverage (Thiel and Madey, 1987; Kurtz and Henrich, 1987). O_2 is inert to hematite {001} at low pressure (Henrich, 1985; Hendewerk et al., 1986; Kurtz and Henrich, 1987). At atmospheric pressure, O_2 chemisorbs and depopulates the Fe-character surface state (Henrich, 1985; Kurtz and Henrich, 1987). As discussed above, this leaves the O 2p states as the highest occupied states and thus explains the absence of Fe in the images taken at negative V_B. The chemisorbed species themselves probably lack electronic states near E_F and so do not appear in the STM images. For example, the MO calculations of Debnath and Anderson (1982) show that O 2p–like states are about 2 eV deeper in the valence band for OH bonded to Fe than for O in an Fe_2O_3-like cluster. Also, photoelectron spectra (Kurtz and Henrich, 1987) show that OH and H_2O contribute to the state density too deep in the valence band (greater than 4 or 5 eV) to contribute to I_T in the STM images in Figure 2. Thus the simple assignment of STM image features to calculated MO states is not always safe because of adsorbate-induced surface states. Gilbert and Kennedy (1989) demonstrated this in a tunneling spectroscopy study of TiO_2 and α-Fe_2O_3 surfaces in air. Most probably, in Figure 2 (at negative V_B), we have imaged states localized on O sites in the top layer of O of the hematite surface (i.e., the sites illustrated in Fig. 1C), and Fe or chemisorbed species above this layer do not contribute to the tunneling current under the imaging conditions used.

Images taken at positive V_B were more variable than those taken at negative V_B. Figure 3A shows peaks in a hexagonal array with 3-Å periodicity, similar to Figure 2. In another image taken in a different area of the same sample (Fig. 3B), an array of triplet peaks appears; the triplets are arranged in a hexagonal array with 5-Å periodicity. An image similar to Figure 3B was obtained by Heil et al. (1989), also at positive (+0.5 V) V_B. Our results suggest that their image is only one of many types of images one may obtain from hematite surfaces under positive V_B conditions, and their assignment of triplet peaks to shared octahedral faces is not a unique interpretation.

Figure 3C gives an example of the most common type of image obtained at positive V_B: single peaks in a hexagonal array with a periodicity of 5 Å (see also STM image in Johnsson et al., 1991). Such images are similar to those obtained using scanning force microscopy (Johnsson et al., 1991), a technique that is not sensitive to LDOS near E_F, as is STM, but to the total electron density. Johnsson et al. (1991) attributed such an array to surface Fe sites. Indeed, only states attributed to equivalent Fe states near the surface could occur in the array imaged in Figure 3C, and both the MO and surface state arguments presented above suggest that the unoccupied states above E_F should have Fe character.

Because the images in Figure 3 were taken during one imaging session with the sample in the same orientation,

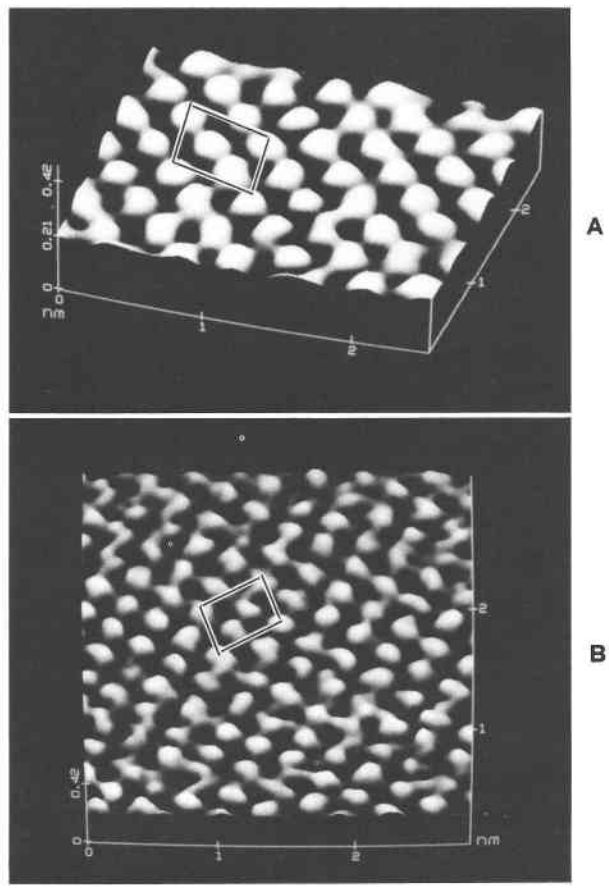

Fig. 2. (**A**), (**B**) Constant-height STM images of hematite {001} taken at −300 mV and 2.2 nA. Peaks occur in a hexagonal array (slightly distorted as a result of drift; see text) with approximately 3-Å periodicity, as characteristic of the surface O array. Unit cells are marked in both images. We show two images to illustrate drift effects; although both images were taken under the same V_B and I_{Tset} conditions, they have different degrees of drift and therefore show slightly different degrees of distortion in the marked surface unit cell, which without drift, would be perfectly hexagonal. The data are displayed in three-dimensional blocks tilted toward the viewer at 30° in **A** and at 60° in **B**. Scales are in nanometers. Both images have been low-pass filtered to remove high-frequency noise.

we may further examine the angular relationships between the peaks in the different images. The peaks (or triplet peaks) in Figures 3B and 3C with 5-Å periodicity (and which therefore indicate some contribution from unoccupied states with Fe character) have similarly oriented hexagonal arrangements. In contrast, the peaks with 3-Å periodicity in Figure 3A are oriented in a hexagonal array that is rotated 30° relative to those in Figures 3B and 3C. This relationship is identical to that expected for Fe vs. O arrays (e.g., compare the arrangement of equivalent Fe sites in Fig. 1C with that of O sites). Thus, it appears that the states to which electrons were tunneling in the different images taken at positive V_B contain differing degrees of Fe and O character; Figure 3A had near-

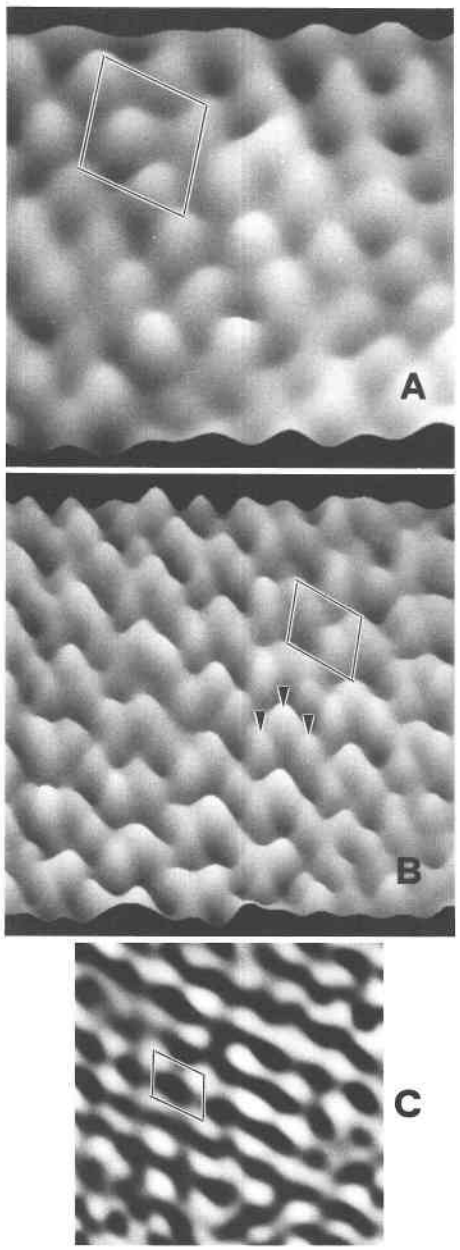

←

Fig. 3. Constant-height STM images of hematite {001} taken at positive V_B; all images are lowpass filtered to remove high-frequency noise. (**A**) An image 19 × 19 Å taken at +1100.8 mV and 2.7 nA; corrugation (relief) in the image is approximately 0.8 Å. Peaks occur in a hexagonal array with roughly 3-Å periodicity, similar to images taken at −300 mV. The data in **A** and **B** are displayed as three-dimensional blocks tilted toward the viewer at 60°. (**B**) An image 38 × 38 Å taken at +1046.8 mV and 5.2 nA; corrugation is approximately 1.0 Å. In this case, peaks occur in triplets (one such triplet is marked with arrows); the triplets occur in a hexogonal array with 5-Å periodicity. (**C**) An image 35 × 35 Å taken at +1099.8 mV and 3.8 nA; corrugation is approximately 0.8 Å. In this case, single peaks occur in a hexagonal array with 5-Å periodicity, as expected for equivalent surface Fe positions. Images **A–C** were taken with the sample in the same orientation, and the 5-Å unit cells marked in the images are all oriented similarly, despite some drift distortion. Note that the subsidiary peaks in each triplet in **B** form lines that are parallel with the rows of O-periodicity sites in **A**.

ly entirely O character, Figure 3B had mixed Fe and O character, and Figure 3C had mostly Fe character. It is not known why different types of images are found at positive V_B, whereas negative V_B consistently gave images like those in Figure 2. It is possible that different tip structures could give rise to different types of images, but this would be likely to affect both positive and negative V_B conditions, not just positive V_B images. Another possibility is that adsorbate-induced surface states might be different in different areas according to local adsorbate coverage or identity. Future STM work may uncover a systematic pattern to positive V_B image variations.

In summary, at this stage, it must suffice to say that positive V_B STM images of hematite {001} are variable, perhaps because of local structural or compositional variations. An important point must be emphasized here, however. Because the unoccupied state density is significant or perhaps dominant in interatomic regions (i.e., the states are not necessarily localized on atomic sites: Tossell et al., 1974; Sherman, 1985), particular peaks cannot be unequivocally assigned to Fe or O atomic sites in the positive V_B images. This is in contrast to the negative V_B images, which show states localized on O sites.

Surface relaxation

In a bulk hematite (001) O plane (see Fig. 1C), two long (3.035 Å) O-O distances alternate with one short (2.669 Å) O-O distance in [210] and equivalent directions. Despite drift (see above), a regular alternation of long and short distances should be observable in STM images. Such a bimodal O-O distance distribution is suggested in Figure 3B for positive V_B conditions, but there are several reasons to be cautious. First, images taken at positive V_B were quite variable and difficult to interpret; second, it is possible that the state density imaged at positive V_B is not localized on atomic positions. Therefore, for purposes of studying O positions in detail, we have used only images taken at negative V_B. Our interpretation is that these images show tunneling current originating from states localized on O sites. The following discussion rests on the assumption that this interpretation is correct.

Figure 4 shows cross sections taken from several images of the surface O array at −300 mV V_B. The distances from peak to peak in each cross section show no obvious systematic alternation of long and short distances. One-dimensional Fourier transforms of the cross sections give single peaks at 2.9 Å. this suggests that the surface O array has relaxed, removing the distortions found in the equivalent bulk plane. However, the error in the measurements must first be shown to be significantly smaller than the proposed relaxation.

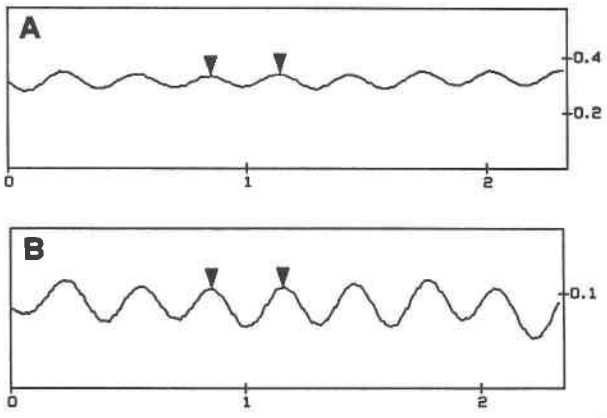

Fig. 4. Cross sections of STM images of hematite {001} taken at −300 mV; scales are in nanometers. (**A**) The triangular cursors mark atoms that are 3.0 Å apart; a one-dimensional fast Fourier transform of this cross section into frequency space gave a single peak at 2.9 Å. (**B**) The triangular cursors mark atoms that are 2.9 Å apart; a one-dimensional fast Fourier transform of this cross section gave a single peak at 2.9 Å. Note that the corrugation (vertical relief) in the two cross sections is similar (approximately 0.5 Å). In an unrelaxed O array in the bulk {001} plane, short (2.7 Å) O-O distances should alternate with long (3.0 Å) distances. No such regular alternation is seen in these cross sections.

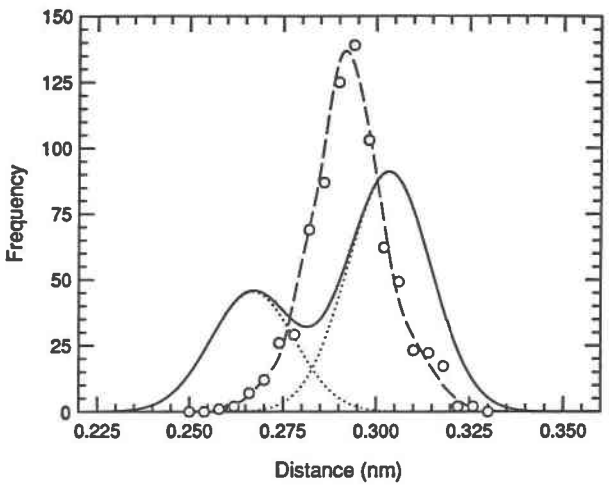

Fig. 5. Frequency distribution for 777 individually measured O-O distances. The measurements were made on six high-resolution STM images taken at −300 mV V_B. The measured distances form a single-mode distribution (dashed line). For comparison, bulk hematite O-O distances in the {001} plane form a bimodal distribution (solid line). The example bimodal distribution is composed of two Gaussian distributions (dotted lines) which were calculated from the standard deviations given by the measured distribution (i.e., the example bimodal distribution is plotted as it would appear if it were subject to the same measurement errors that the observed single-mode distribution was subject to, except that the measured distribution is not perfectly Gaussian). Surface O-O distances apparently do not retain the bimodal distribution characteristic of the bulk.

A problem with measuring distances directly from the STM images is the systematic error introduced by drift effects (see above). Drift may distort the surface unit-cell symmetry as displayed in an STM image, causing distances to be too small in one direction and too large in another direction. Drift effects can be accounted for by recognizing that the average O-O distance would be 2.913 Å in the unrelaxed bulk hematite (001) plane as well as in a relaxed (regularized) surface array but that the distribution of O-O distances would be bimodal for the unrelaxed surface and single mode for the relaxed surface. We removed systematic drift error as follows:

Step 1: Measure individual O-O distances (designated X) from STM images, making sure to group only measurements made in a particular direction (direction is designated by the index i). The resulting data consist of a number n_i of measurements X_i. Step 2: For each data set i, calculate $X_i^{ave} = (\Sigma X_i)/n_i$. Step 3: Because of drift, generally X_i^{ave} is not equal to 2.913 Å. This discrepancy is due to drift error because LEED results (Hochella et al., 1989) show that the surface unit cell is not different in size from the bulk structure in the (001) plane. Therefore, we calculate a scaling facter S_i where $S_i = X_i^{ave}/(2.913)$. Then, for each X_i, we calculate $X_i(S_i)$. By definition, $\{\Sigma[X_i(S_i)]\}/n_i = 2.913$ Å. As a result, the numbers $X_i(S_i)$ are comparable for different i because drift effects have been removed, so the data for different directions i can be collected into one data set and plotted as number of observations vs. drift-corrected O-O distance.

The frequency distribution resulting from the above procedure is plotted in Figure 5. The O-O distances form a single-mode distribution. For comparison, peaks reflecting the bimodal distribution of O-O distances in the bulk (001) plane are plotted as Gaussian curves whose peak widths are calculated from the standard deviations of the measured distribution (which was not exactly Gaussian). The measured single-mode distribution is sufficiently narrow that it could not mask a bimodal distribution, even with the substantial measurement errors. Again, this supports the idea that the surface O array has relaxed away from the distorted bulk structure (which would give the bimodal distribution) to a more regular array (giving the observed single-mode distribution).

Surface relaxation: Consistency with surface forces

In this section we consider a simple, qualitative model of the forces acting on surface O atoms in relation to the relaxations suggested by our observations.

Although ionic attraction and repulsion are significant over distances of 10 Å or more in an ionic crystal (Smyth, 1989), their strength decays with the square of the distance, and consideration of nearest-neighbor Fe and O should serve to form a useful qualitative picture of the forces acting on an O site at a surface. For purposes of qualitative argument, we may think of Fe-O interactions as approximated by a Lennard-Jones-type potential in which Fe-O bond lengths less than the length of an un-

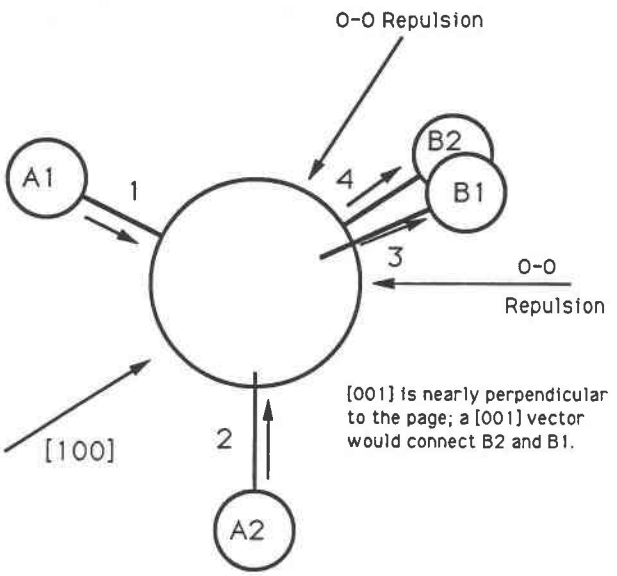

Fig. 6. Model of a single O site, together with arrows indicating the direction of forces exerted on the O by its first coordination sphere of Fe and by nearest-neighbor O. This site corresponds to the site marked A in Figure 1C. Fe sites A1 and B2 are below the plane of the page, and sites A2 and B1 are above the plane of the page. Bonds labeled 1 and 2 are short relative to unstrained Fe-O bonds and exert repulsive net forces on the O; bonds labeled 3 and 4 are long relative to unstrained Fe-O bonds and exert attractive forces on the O. The net force vector points in the [100] direction. This force is balanced by O-O repulsion (the two arrows indicating O-O repulsion indicate the direction of short O-O distances in the bulk (001) plane). If the Fe labeled B1 is removed, as is likely during the creation of a {001} surface, the net force due to Fe-O interaction will be reduced and the O should relax back along [$\bar{1}$00] in response. Such relaxation would result in a regularized surface array because the O relaxes away from its closest O neighbors.

distorted bond (about 2.06 Å; see above) should give net repulsive forces between Fe and O, and Fe-O bond lengths greater than 2.06 Å should give net attractive forces between Fe and O. O-O repulsion can be approximated by an ionic potential, which always gives repulsive forces between O ions. Figure 6 shows an O atom, together with the four Fe atoms that coordinate it, plucked from the hematite bulk structure. To place this O atom in its structural context, it is equivalent to the one marked A in Figure 1C.

Of course, the forces exerted on an atom in a bulk structure are balanced, i.e., the position around which an atom vibrates represents a local minimum in its potential field. Considering the O atom in Figure 6, we see qualitatively that the short Fe-O bonds (marked 1 and 2) both exert repulsive forces on the O, and long Fe-O bonds (marked 3 and 4) both exert attractive forces on the O; the net force on the O from Fe-O interaction is in the [100] direction. In the bulk structure, these forces are counteracted by repulsion between the O and its neighboring O atoms; the short O-O distances (see Fig. 1C) exert forces in the opposite direction [$\bar{1}$00]. This simple picture is consistent with the thermal ellipsoids for hematite calculated in Blake et al. (1966); for O, the thermal ellipsoid is elongated toward the vacant octahedral site, which is precisely the direction along which force gradients are lowest in Figure 6.

We may now consider what would happen to this balance if the Fe marked B1 were removed, leaving behind only the low Fe on the surface (see above). The pull exerted by B1 would be removed, resulting in a net force on the O back along the [$\bar{1}$00] direction as well as down into the surface slightly. Chemisorption of H_2O and O to coordinate the remaining surface Fe atoms might alter this situation, but would probably not inhibit relaxation; the low Fe (A2) exerts a push on the O because of Fe-Fe repulsions between face-sharing octahedra that push the Fe down against the O atoms. Because surface Fe (A2) is no longer face sharing, but coordinated by O, H_2O, or perhaps other adventitious species, the push exerted by it on the central O would be expected to decrease, which would also contribute to O relaxation back along [$\bar{1}$00] as well as allow the Fe (A2) to relax upward along [001].

Because all O positions are symmetrically equivalent, the arguments presented above apply to all surface O atoms. Therefore, it appears that a regularization of the surface O array is consistent with a simple comparison of forces acting on O atoms at surfaces relative to the forces in the bulk structure. The above arguments show that the relaxation we proposed is essentially the result of removing, at the surface, the distortion in the O array caused by face sharing of Fe octahedra in the bulk structure. O relaxation as described above would also result in slight rotation of the large O triangles in the surface O array (see Fig. 1C); this is because O atoms would relax along [100] and equivalent directions, whereas the direction of nearest-neighbor O atoms on a (001) plane are along [210] and equivalent directions (see Fig. 7).

An accurate accounting of the likely magnitude of the effect of surface relaxation on the surface energy of hematite {001} would require knowing the exact extent of relaxation both laterally and vertically, accurate potential functions for both Fe-O and O-O interactions, and the effects of chemisorbed species on relaxation. Although such information is unavailable, we anticipate that the small shifts required to make a regularized array could be responsible only for a few percent reduction in surface energy from that of an unrelaxed surface structure, simply because such small shifts produce small changes in energy relative to the energy required to break a bond.

Microtopography

Steps varying in height from 2.3 Å (corresponding to one O layer) to several nanometers (several unit cells) were frequently observed on hematite {001} parting surfaces. Steps occur parallel to visible striations and edges on hematite parting surfaces, and when imaged at the atomic scale are found to occur parallel to [210] and equivalent directions. At moderate resolution, flat sur-

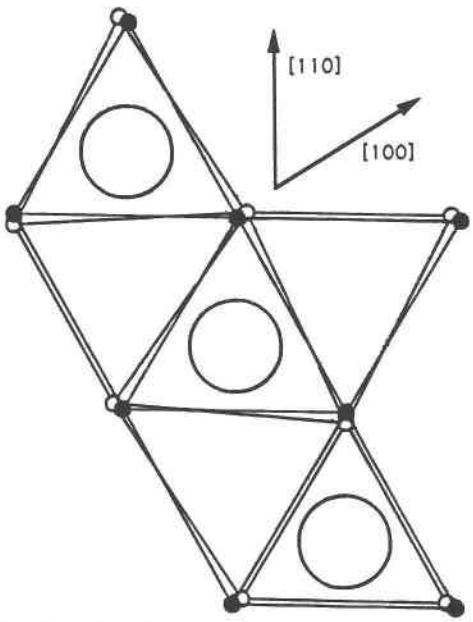

Fig. 7. A model of a small segment of the hematite {001} surface. Unfilled small circles represent O positions in the unrelaxed bulk {001} plane. Filled small circles represent O positions in a perfectly regular surface O array, as suggested by the STM images. Large open circles represent Fe positions above or below the O plane. Note that relaxation expands the shared octahedral face (lower part of the figure) and slightly rotates the larger, unshared octahedral faces (upper part of the figure).

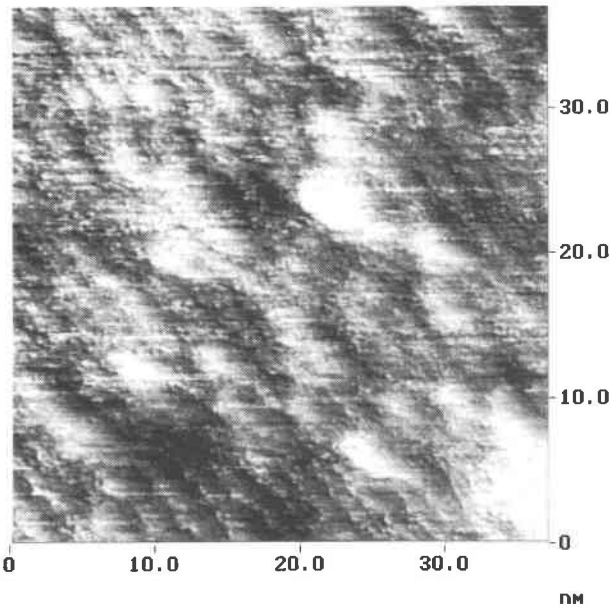

Fig. 8. A constant-height STM image of steps on a hematite {001} parting surface, taken at −300 mV and 1.5 nA. The scale is in nanometers. The horizontal streaks are a rastering artifact. Despite the noise in the image, steps can be seen that trend from upper left to lower right. It is apparent that the step density is large, with steps spaced approximately every 20–30 Å. High-resolution images taken near this area are presented in Figures 9 and 11.

faces (surfaces that, for example, would appear flat in an SEM image) were found to have step spacings of roughly 2–3 nm (Fig. 8). Edge energies associated with step edges on surfaces with such high step densities might be expected to contribute to the overall surface energy (e.g., Williams and Bartelt, 1991), and the unique coordination environments of step-edge and kink sites might occur in sufficiently high concentration to play a key role in hematite surface reactivity.

Figure 9 is a high-resolution STM image of two successive steps spaced approximately 25 Å apart. This image was taken at −300 mV V_B and thus shows states localized on O positions (see above). The "up" and "down" sides of the steps can be discerned if one considers the imaging mechanism; Figure 9 is an image of tunneling current (I_T) variation taken with the tip scanning at essentially constant height from right to left. Running the feedback loop at low gain settings allows for control of the average tip-sample separation over lateral distances in the 1–2 nm range but gives little z-piezo response to tunneling current variations on the atomic scale. When the tip, scanning from right to left, reaches a step down, I_T drops drastically because the tip-sample separation increases by a few angstroms. In response, the feedback loop gradually moves the tip closer to the sample over a distance of about 2 nm (in this case) in order to keep the average I_T constant, i.e., maintain constant height. Therefore, the steps in Figure 9 step down from upper right to lower left. Unfortunately, the atomic structure on the immediate down side of each step is often lost as the tip position equilibrates; also, because these surfaces have been exposed to air, adsorbates may be segregated along steps and affect I_T, both by intervening between tip and sample and by altering the local electronic structure.

Figure 10 is a model of a step; the line labeled 1 illustrates the offset of O rows as one goes from terrace to terrace. In Figure 9, the line labeled 1 shows this offset in the STM image. In addition, the regular O row spacings appear to be interrupted at the step edge. The distance between the atomic rows marked 2 and 3 (the rows nearest the step edge) in Figure 9 is 1.5 times larger than the usual row spacing on a terrace; there is also a dimly visible row between the rows marked 2 and 3. A similar situation exists for the second step with rows marked 4 and 5, except that the row between 4 and 5 is bright rather than dim.

The "ideal" step illustrated in Figure 10 shows fivefold-coordinated Fe sites and that two occupied Fe sites alternate with single vacant sites (marked with arrows) along the step. O sites at the ideal step edge occur in triplets; e.g., see the groups of three O atoms along the step edge and between the black arrows in Figure 10. In each O triplet, the two O atoms on the ends are only twofold coordinated and the middle O is threefold coordinated. Thus, the fivefold-coordinated Fe sites at steps are more bulklike than on terraces, and two-thirds of the

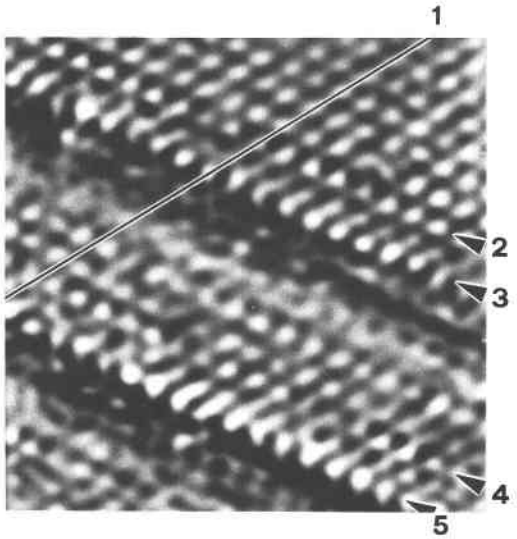

Fig. 9. A constant-height STM image, 54 × 54 Å, of two steps on a hematite {001} parting surface, taken at −300 mV and 1.5 nA. Terraces step down from upper right to lower left (see text). The height of each step is approximately 2.5 Å, based on variation in tunneling current. The line labeled 1 shows the offset of O rows on terraces of different elevation (see Fig. 10). The step structure is different from the terrace structure; the spacing of the rows labeled 2 and 3 and of the rows labeled 4 and 5 is 1.5 times the normal spacing of O rows. Between rows 2 and 3 and between rows 4 and 5 is a row of sites that is poorly resolved and whose origin is not understood. The steps appear to be relaxed or reconstructed.

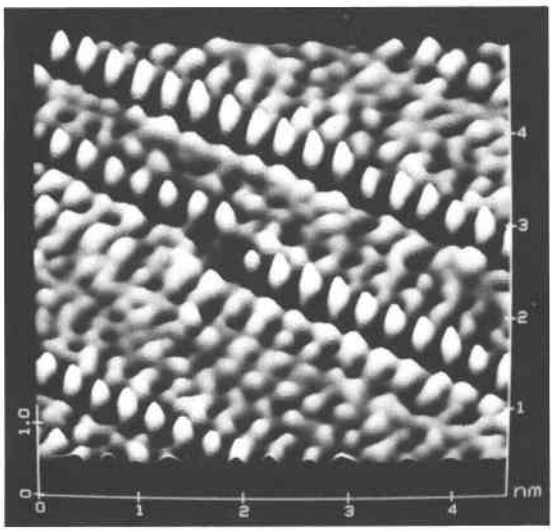

Fig. 11. A constant-height STM image taken only a few nanometers away from the area imaged in Figure 9. The data are displayed in a three-dimensional block tilted toward the viewer at 60°. Total relief is approximately 10 Å. A kink site appears near the center of the image. Terraces step down from upper right to lower left. The sites along each step edge appear as taller bumps than sites on terraces, indicating a difference in electronic structure, O position, or both at step edges as compared with terrace sites.

O sites are less coordinated than on terraces. Coordinative undersaturation would tend to destabilize the occupied O 2p–like states near the top of the valence band, raising their energy (e.g., Sherman, 1985). In an STM image, this would result in brighter sites at step edges relative to sites within terraces. In Figure 9, there is some evidence that sites at the step edges are brighter than those on terraces, especially in row 5, but there is no evidence for an alternation of two-bright, one-dark sites as suggested by the above arguments.

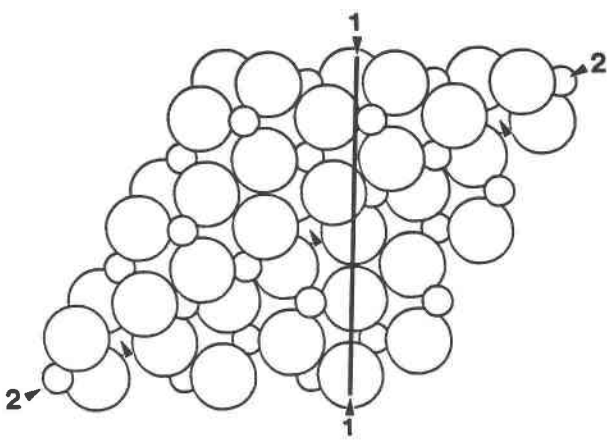

Fig. 10. A model of a step on a hematite {001} surface. The offset of O rows on the terraces above and below the step is illustrated by the line labeled 1. Along a row of Fe atoms at a step (labeled 2), Fe vacancies occur at every third site (marked with arrows). Along the step, between Fe vacancies, O atoms occur in triplets (see text).

The bright spots at the step edge in Figure 9 occur in positions that appear to be directly over the Fe sites at the step (i.e., the row of Fe marked 2 in Fig. 10). One possibility is that, because O-O repulsion is unbalanced at the step edge, O may relax away from the step and occupy sites above Fe atoms. Although such relaxation may indeed occur at steps, neither this nor the previous argument explains the dim rows between rows 2 and 3 and between rows 4 and 5 in Figure 9. Also, such relaxation would differ for twofold- and threefold-coordinated O atoms along the step, and no evidence of periodic alternation of sites is apparent along the step edges in Figure 9.

These arguments illustrate one difficulty of STM image interpretation, namely, that electronic and atomic structure information is intimately convolved. We cannot tell, for example, to what extent the extra brightness of step edge sites is due to the atoms being physically higher (perhaps because of relaxation at the step edge) and to what extent the extra brightness is due to shifts in electronic structure. Our arguments explain some of, but not all of, the features of steps in STM images. Without independent information on the location of Fe in relation to O and on the potential role of adsorbates in altering local geometric and electronic structure at the step, a sin-

gle model cannot be proven. For example, Becker and Vickers (1990) point out in their STM study of steps on As-terminated Ge (111) surfaces that one must be particularly cautious in interpreting STM images of steps and other one-dimensional structures. They were unable to achieve an unequivocal correspondence between several proposed step models (and attendant electronic structure calculations) and their STM data.

Figure 11 was taken only a few nanometers away from the area imaged in Figure 9, except with different gain settings. The steps in this image again step down from upper right to lower left. The higher gain settings cause the tip to overshoot as it corrects for changes in tip-sample separation at steps. This overshoot often causes an oscillation that swamps the atomic structure on the terraces when steps are closely spaced, as in this case. Figure 11 again shows the reconstruction of the step edge and, in addition, shows a kink site in one of the steps. The ability to image kink sites should prove valuable in the future, as kink sites may often be important in overall surface reactivity. The atoms along the step edges in Figure 11 again appear to be higher than those on terraces, in agreement with the destabilization of O 2p states along step edges discussed above. Although we cannot solve the reconstructed step structure on the basis of these STM images, the above discussion suggests that O sites are most likely to be perturbed at step edges, either by changing positions or by changing electronic structure, and probably by both effects.

At present, it must suffice to say that the STM images show strong evidence for relaxation or reconstruction at step edges, but the precise nature of the structural changes is not clear. In any case, such a reconstruction could have important implications for hematite reactivity. Elucidation of step structures appears to be a useful goal for future STM studies of hematite and other minerals.

Conclusions

In summary, we have interpreted STM data for hematite {001} surfaces in relation to calculated and experimentally investigated electronic structures. Using our interpretation, we discussed features of hematite surfaces, such as relaxation and step structure. We wish to emphasize that STM images show the distribution of electronic state density at surfaces. STM images can be used with confidence to investigate atomic structures only if independent electronic structure information can be used to form an understanding of how electronic states are likely to be distributed.

Acknowledgments

This research was supported by the Petroleum Research Fund of the American Chemical Society (22892-ACS,2 to M.F.H.), the National Science Foundation (EAR-9105000 to M.F.H.), and the McGee Fund of the School of Earth Sciences at Stanford (to C.M.E.). We also thank the Center for Materials Research at Stanford for research and instrumentation support. C.M.E. acknowledges the constructive influence of the late Noye M. Johnson of Dartmouth College, and the support of Werner Stumm, Barbara Sulzberger, and the Swiss Federal Institute for Water Resources and Water Pollution Control (EAWAG). Virgil Elings and Kevin Kjoller provided helpful information on the Digital Instruments Nanoscope II hardware and software. We thank Susan Stipp, Patricia Johnsson, George Parks, Gordon Brown, Jr., and Jodi Junta for helpful comments and discussions, and an anonymous reviewer for comments.

References cited

Adamson, A.W. (1982) Physical chemistry of surfaces (4th edition), 664 p. Wiley, New York.

Avouris, Ph. (1990) Atom-resolved surface chemistry using the scanning tunneling microscope. Journal of Physical Chemistry, 94, 2246–2256.

Becker, R., and Vickers, J. (1990) Determination of surface atomic positions by scanning tunneling microscope observations. Journal of Vacuum Science and Technology, A8 (1), 226–232.

Benson, G.C., and Yun, K.S. (1967) Surface energy and surface tension of crystalline solids. In E.A. Flood, Ed., The solid gas interface, p. 203–269. Marcel-Decker, New York.

Blake, R.L., Hessevick, R.E., Zoltai, T., and Finger, L.W. (1966) Refinement of the hematite structure. American Mineralogist, 51, 123–129.

Bolt, G.H., and Van Riemsdijk, W.H. (1987) Surface chemical processes in soil. In W. Stumm, Ed., Aquatic surface chemistry, p. 127–164. Wiley, New York.

Brantley, S.L., Crane, C.F., Crerar, D.A., Hellmann, R., and Stallard, R. (1986) Dissolution at dislocation etch pits in quartz. Geochimica et Cosmochimica Acta, 50, 2349–2361.

Brown, G.E., Jr. (1990) Spectroscopic studies of chemisorption reaction mechanisms at oxide-water interfaces. In Mineralogical Society of America Reviews in Mineralogy, 23, 309–363.

Causa, M., Dovesi, R., Pisani, C., and Roetti, C. (1989) Ab initio characterization of the (0001) and (1010) crystal surfaces of α-alumina. Surface Science, 215, 259–271.

Chang, C.C. (1968) LEED studies of the (0001) face of α-alumina. Journal of Applied Physics, 39 (12), 5570–5573.

Charig, J.M. (1967) Low energy electron diffraction observation of α-alumina. Applied Physics Letters, 10, 139–140.

Debnath, N.C., and Anderson, A.B. (1982) Optical spectra of ferrous and ferric oxides and the passive film: A molecular orbital study. Journal of the Electrochemical Society, 129 (10), 2169–2174.

Eggleston, C.M., and Hochella, M.F., Jr. (1990) Scanning tunneling microscopy of sulfide surfaces. Geochimica et Cosmochimica Acta, 54, 1511–1517.

——— (1991) Scanning tunneling microscopy of galena (100) surface oxidation and sorption of aqueous gold. Science, 254, 983–986.

Fasiska, E.J. (1967) Structural aspects of the oxides and oxyhydrates of iron. Corrosion Science, 7, 833–839.

French, T.M., and Somorjai, G.A. (1970) Composition and surface structure of the (0001) face of α-alumina by low energy electron diffraction. Journal of Physical Chemistry, 74 (12), 2489–2495.

Giese, J.R.F. (1974) Surface energy calculations for muscovite. Nature, 248, 580–581.

Gilbert, S.E., and Kennedy, J.H. (1989) Observation of hysteresis induced by the tip field in scanning tunneling microscope spectroscopic probing of TiO_2 and α-Fe_2O_3 single crystal surfaces. Langmuir, 5, 1412–1415.

Heil, J., Wesner, J., Lommel, B., Assmus, W., and Grill, W. (1989) Structural investigation of blue bronzite and hematite by scanning tunneling microscopy. Journal of Applied Physics, 65 (12), 5220–5222.

Hendewerk, M., Salmeron, M., and Somorjai, G.A. (1986) Water adsorption on the (001) plane of Fe_2O_3: An XPS, UPS, Auger, and TPD study. Surface Science, 172, 544–556.

Henrich, V.E. (1985) The surfaces of metal oxides. Reports on Progress in Physics, 48, 1481–1541.

Hochella, M.F., Jr. (1990) Atomic structure, microtopography, composition, and reactivity of mineral surfaces. In Mineralogical Society of America Reviews in Mineralogy, 23, 87–132.

Hochella, M.F., Jr., Eggleston, C.M., Elings, V.B., Parks, G.A., Brown, G.E., Jr., Wu, C.M., and Kjoller, K.K. (1989) Mineralogy in two dimensions: Scanning tunneling microscopy of semiconducting minerals with implications for geochemical reactivity. American Mineralogist, 74, 1233–1246.

Hochella, M.F., Jr., Eggleston, C.M., Elings, V.B., and Thompson, M.S.

(1990) Atomic structure and morphology of the albite (010) surface: An atomic force microscope and electron diffraction study. American Mineralogist, 75, 723–730.

Jaycock, M.J., and Parfitt, G.D. (1981) Chemistry of interfaces. Wiley, New York.

Johnsson, P.A. Eggleston, C.M., and Hochella, M.F., Jr. (1991) Imaging molecular-scale structure and microtopography of hematite with the atomic force microscope. American Mineralogist, 76, 1442–1445.

Kurtz, R.L., and Henrich, V.E. (1983) Geometric structure of the α-Fe_2O_3 (001) surface: A LEED and XPS study. Surface Science, 129, 345–354.

——— (1987) Surface electronic structure and chemisorption on corundum transition metal oxides: α-Fe_2O_3. Physical Review B, 36 (6), 3413–3421.

Lasaga, A.C., and Blum, A.E. (1986) Surface chemistry, etch pits and mineral-water reactions. Geochimica et Cosmochimica Acta, 50, 2363–2379.

Lawn, B.R., and Wilshaw, T.R. (1975) Fracture of brittle solids. Cambridge Solid State Science Series. Cambridge University Press, Cambridge, U.K.

Leland, J.K., and Bard, A.J. (1987) Photochemistry of colloidal semiconducting iron oxide polymorphs. Journal of Physical Chemistry, 91, 5076–5083.

Lindsley, D.H. (1976) The crystal chemistry and structure of oxide minerals as exemplified by the Fe-Ti oxides. In Mineralogical Society of America Reviews in Mineralogy, 3, L1–L60.

Parks, G.A. (1984) Surface and interfacial free energies of quartz. Journal of Geophysical Research, 89 (B6), 3997–4008.

——— (1990) Surface energy and adsorption at mineral/water interfaces: An introduction. In Mineralogical Society of America Reviews in Mineralogy, 23, 133–175.

Pisani, C., Causa, M., Dovesi, R., and Roetti, C. (1987) Hartree-Fock ab-initio characterization of ionic crystal surfaces with a slab model. The (001) face of α-Al_2O_3. Progress in Surface Science, 25, 119–137.

Schneir, J., and Hansma, P.K. (1987) Scanning tunneling microscopy and lithography of solid surfaces covered with non-polar liquids. Langmuir, 3, 1025–1027.

Schwertmann, U., and Taylor, R.M. (1977) Iron oxide. In J.B. Dixon and S.B. Weed, Eds., Minerals and soil environments, p. 145–180. Soil Science Society of America, Madison, Wisconsin.

Sherman, M.J. (1985) The electronic structures of Fe^{3+} coordination sites in iron oxides; applications to spectra, bonding, and magnetism. Physics and Chemistry of Minerals, 12, 161–175.

Shuey, R.T. (1975) Semiconducting ore minerals, 415 p. Elsevier, Amsterdam.

Smyth, J. (1989) Electrostatic characterization of oxygen sites in minerals. Geochimica et Cosmochimica Acta, 53, 1101–1110.

Somorjai, G.A. (1981) Chemistry in two dimensions: Surfaces, 575 p. Cornell University Press, Ithaca, New York.

Sparnaay, M.J. (1985) Thermodynamics (with emphasis on surface problems). Surface Science Reports, 4, 101–269.

Stumm, W., and Sulzberger, B. (1992) The cycling of iron in natural environments; considerations based on laboratory studies of heterogeneous processes. Geochimica et Cosmochimica Acta, in press.

Susnitzky, D.W., and Carter, C.B. (1984) Identification of α-alumina surface structures by electron diffraction. Journal of the American Ceramics Society, 69 (9), C-217–C-220.

Thiel, P.A., and Madey, T.E. (1987) The interaction of water with solid surfaces: Fundamental aspects. Surface Science Reports, 7, 211–385.

Tossell, J.A., Vaughan, D.J., and Johnson, K.H. (1973) The electronic structure of ferric iron octahedrally coordinated to oxygen: A fundamental polyhedral unit of iron-bearing oxide and silicate minerals. Nature, 244, 42–45.

——— (1974) The electronic structure of rutile, wustite, and hematite from molecular orbital calculations. American Mineralogist, 59, 319–334.

Waite, T.D. (1990) Photo-redox processes at the mineral-water interface. In Mineralogical Society of America Reviews in Mineralogy, 23, 559–603.

Williams, E.D., and Bartelt, N.C. (1991) Thermodynamics of surface morphology. Science, 251, 393–400.

Zhang, J.D., and Nancollas, G.H. (1990) Mechanisms of growth and dissolution of sparingly soluble salts. In Mineralogical Society of America Reviews in Mineralogy, 23, 365–396.

Manuscript received November 18, 1991
Manuscript accepted May 11, 1992